Preprint
UCRL-JC-145156

Time-Reversal Acoustics and Maximum-Entropy Imaging

James G. Berryman
Lawrence Livermore National Laboratory

This article was submitted to 142nd Meeting of the Acoustical Society of America Conference, Fort Lauderdale, FL, December 3-7, 2001

U.S. Department of Energy
Lawrence Livermore National Laboratory

August 22, 2001

UCRL-JC-

Version date: August 22, 2001

Time-Reversal Acoustics and Maximum-Entropy Imaging

James G. Berryman
University of California
Lawrence Livermore National Laboratory
P. O. Box 808 L-200
Livermore, CA 94551-9900

Abstract

Target location is a common problem in acoustical imaging using either passive or active data inversion. Time-reversal methods in acoustics have the important characteristic that they provide a means of determining the eigenfunctions and eigenvalues of the scattering operator for either of these problems. Each eigenfunction may often be approximately associated with an individual scatterer. The resulting decoupling of the scattered field from a collection of targets is a very useful aid to localizing the targets, and suggests a number of imaging and localization algorithms. Two of these are linear subspace methods and maximum-entropy imaging.

PACS numbers: 43.20.Fn, 43.30.Gv

1 Introduction

Time-reversal acoustics (Fink, 1997; 1999) has become an important research area in recent years because of the many potential applications associated with it and envisioned for it. In biomedical applications, the prototype is the detection and destruction of kidney stones by ultrasound. By insonifying the kidney with pulses of ultrasound and measuring the return signal, it is possible to localize one or more kidney stones and then to send a return signal back to the scatterer with high enough amplitude to cause the stone to fragment, and the remaining pieces then eventually to pass harmlessly from the system. Training the sound to find the kidney stone automatically is the main function of time-reversal acoustics in this application. Analyses of why it works so well and means of improving its performance have been studied by many authors (Prada *et al.*, 1991; 1995; Prada and Fink, 1994; Mast *et al.*, 1997; Devaney, 1999; Blomgren *et al.*, 2001; Tsogka and Papanicolaou, 2001). Most of these analyses have concentrated on focusing on or imaging of small point-like targets.

Chambers and Gautesen (2001) have recently shown that a single extended spherical acoustic scatterer has from two to four eigenfunctions associated with it. To understand this result, it might help to put it in a larger context by considering scattering from a single spherical elastic scatterer imbedded in an otherwise homogeneous elastic medium. Then, it is well-known that the principal scattering terms arise from changes in bulk modulus (K), density (ρ), and shear modulus (μ). Bulk modulus changes produce monopole scattering; density changes produce dipole scattering; and shear modulus changes produce quadrupole scattering. There is at most one contribution from monopole scattering; at most three from dipole scattering; and, for acoustics, there is no quadrupole scattering, as there are no viable shear waves. The scattering multiplicity found by Chambers and Gautesen is then understood as, at most $1 + 3 = 4$, while some of the dipole terms may not be excited because of the scatterer-to-sensor array orientation. The monopole term is the one usually treated in analyses of time-reversal acoustics, but for some situations — such as air bubbles in liquid — the dipole terms should also be considered. Nevertheless, we will only consider the monopole contributions in this paper. The generalization of the methods to be presented here in order to incorporate other modes is actually straightforward, as we shall see, and, except for the fact that the trial vectors used for imaging must be tailored to these other modes, the analysis proceeds without any significant alteration.

The fundamental concepts used in time-reversal imaging for acoustics are closely related to concepts in optimal probing and imaging for a variety of physical problems including work by

Isaacson (1986), Gisser *et al.* (1990), Cherkaeva and Trip (1996a,b), Colton and Kirsch (1996), Kirsch (1998), and Brühl *et al.* (2001).

Section 2 presents a review of the relevant issues in acoustic scattering and time-reversal signal processing. Section 3 discusses the linear subspace methods of imaging including the well-known MUSIC algorithm, as well as some modifications of MUSIC, and related algorithms. Section 4 introduces the maximum-entropy imaging approach which is often the preferred method when data are sparse. Section 4 also gives examples and Section 5 discusses our conclusions.

2 Acoustic Scattering and Time Reversal

Time-reversal acoustics can be studied either in the time domain or in the frequency domain. The two domains have complementary advantages and disadvantages.

Pluses and minuses for the time domain include: Acoustical experiments are generally performed in the time domain. Self-focusing in any acoustic medium can be achieved using time-reversal processing in the time domain. Delay-time windowing easily distinguishes arrivals from well-separated scatterers in the time domain. But, if we want to understand the eigenvector/eigenvalue structure of the acoustic scattering operator in the time domain, we can only obtain one eigenvector at a time, and to obtain more eigenvectors (after the first one) a rigorous orthogonalization procedure must be followed.

Advantages of the frequency domain include the fact that eigenvector/eigenvalue or singular value decomposition (SVD) is quite easily done in the frequency domain, although it is then done one frequency at a time. Thus, all eigenvalues/eigenvectors or singular values/singular vectors are obtained simultaneously. Linear subspace imaging methods are then also most easily applied in the frequency domain. The main disadvantage of the frequency domain is that it is not simple to take advantage of target separation in space (and therefore in time) in this domain.

We will return to discuss more about time domain processing later in the paper, but for now we assume that all measured time traces have been Fourier transformed into the frequency domain, and that the pertinent equation to study is therefore the Helmholtz equation.

2.1 Acoustic wave scattering

We assume that the problems of interest are well-approximated by the inhomogeneous Helmholtz equation

$$\left[\nabla^2 + k_0^2 n^2(\mathbf{x})\right] u(\mathbf{x}) = s(\mathbf{x}), \tag{1}$$

where $u(\mathbf{x})$ is the wave amplitude, $s(\mathbf{x})$ is a localized source function, $k_0 = \omega/c_0 = 2\pi f/c_0 = 2\pi/\lambda$ is the wavenumber of the homogeneous background, with ω being angular frequency, f frequency, c_0 the assumed homogeneous background wave speed, and λ wavelength. The acoustic index of refraction is

$$n(\mathbf{x}) = \frac{c_0}{c(\mathbf{x})}, \tag{2}$$

where $c(\mathbf{x})$ is the wave speed at spatial location $\mathbf{x}$. Thus, $n^2(\mathbf{x}) = 1$ in the background and

$$a(\mathbf{x}) = n^2(\mathbf{x}) - 1 \tag{3}$$

measures the change in the wave speed at the scatterers.

Pertinent fundamental solutions for this problem satisfy:

$$\left[\nabla^2 + k_0^2\right] G_0(\mathbf{x}, \mathbf{x}') = -\delta(\mathbf{x} - \mathbf{x}') \tag{4}$$

and

$$\left[\nabla^2 + k_0^2 n^2(\mathbf{x})\right] G(\mathbf{x}, \mathbf{x}') = -\delta(\mathbf{x} - \mathbf{x}'), \tag{5}$$

for the homogeneous and inhomogeneous media, respectively. In both cases, we assume the radiation (out-going) boundary condition at infinity.

The well-known solution of (4) for the homogeneous medium in 3D is

$$G_0(\mathbf{x}, \mathbf{x}') = \frac{e^{ik_0|\mathbf{x}-\mathbf{x}'|}}{4\pi|\mathbf{x} - \mathbf{x}'|}. \tag{6}$$

The fundamental solution of (5) for the inhomogeneous medium can be written in terms of that for the homogeneous one (in the usual way) as

$$G(\mathbf{x}, \mathbf{x}') = G_0(\mathbf{x}, \mathbf{x}') + k_0^2 \int a(\mathbf{y}) G_0(\mathbf{x}, \mathbf{y}') G(\mathbf{y}, \mathbf{x}')\, d^3y. \tag{7}$$

Note that the right hand side depends on the values of the G, which is to be determined by the same equation. So this is an implicit integral equation that must be solved for $G(\mathbf{x}, \mathbf{x}')$. The regions of nonzero $a(\mathbf{y})$ are assumed to be finite in number (N), in compact domains Ω_n, all of which are small compared to the wavelength λ. Then, there will be some position $\mathbf{y}_n$ (certainly for convex domains) inside each domain Ω_n, characterizing the location of each of the N scatterers. We also call these scatterers "targets," since it is their locations that we seek.

With these assumptions, it is a good approximation to set the $\mathbf{y}$ arguments of G_0 and G inside the integral equal to $\mathbf{y}_n$ for all $\mathbf{y}$'s inside domain Ω_n. Then, the fundamental solutions can be moved outside of the integral. There remains the integral over $a(\mathbf{y})$, incorporated into the scattering coefficient

$$q_n \equiv k_0^2 \int_{\Omega_n} a(\mathbf{y})\, d^3y, \tag{8}$$

which then characterizes the strength of the scattering from the nth target domain.

With these definitions, we finally have

$$G(\mathbf{x}, \mathbf{x}') \simeq G_0(\mathbf{x}, \mathbf{x}') + \sum_{n=1}^{N} q_n G_0(\mathbf{x}, \mathbf{y}_n) G(\mathbf{y}_n, \mathbf{x}'). \tag{9}$$

Furthermore, if the scatterers are sufficiently far apart and the scattering strengths q_n are not too large, then $G(\mathbf{y}_n, \mathbf{x}')$ on the far right can be replaced by $G_0(\mathbf{y}_n, \mathbf{x}')$, giving the explicit formula

$$G(\mathbf{x}, \mathbf{x}') \simeq G_0(\mathbf{x}, \mathbf{x}') + \sum_{n=1}^{N} q_n G_0(\mathbf{x}, \mathbf{y}_n) G_0(\mathbf{y}_n, \mathbf{x}'). \tag{10}$$

Equation (10) is the Born approximation to $G(\mathbf{x}, \mathbf{x}')$ for small scatterers.

2.2 Acoustic time-reversal data analysis

Time-reversal acoustics can be understood in a straightforward way from the scattering theory presented so far. First, define a complex vector $\mathbf{H}_n$ relating scattering at point $\mathbf{y}_n$ with all M of the acoustic sensors in a sensor array located at positions $\mathbf{x}_1, \mathbf{x}_2, \ldots, \mathbf{x}_M$. Then,

$$\mathbf{H}_n^T = \left(G_0(\mathbf{y}_n, \mathbf{x}_1) \quad \ldots \quad G_0(\mathbf{y}_n, \mathbf{x}_M) \right). \tag{11}$$

By analogy to (11), we define a general vector of the same form $\mathbf{H}_r$, indexed by a general location in the model space $\mathbf{r}$, such that

$$\mathbf{H}_r^T = \left(G_0(\mathbf{r}, \mathbf{x}_1) \quad \ldots \quad G_0(\mathbf{r}, \mathbf{x}_M) \right). \tag{12}$$

We will term $\mathbf{H}_r$ a "trial vector" at $\mathbf{r}$, and $\mathbf{H}_n$ one of the set of N "solution vectors."

With these definitions, the fundamental solution in the Born approximation can be rewritten for $m, m' = 1, \ldots, M$ as

$$G(\mathbf{x}_m, \mathbf{x}_{m'}) \simeq G_0(\mathbf{x}_m, \mathbf{x}_{m'}) + K(\mathbf{x}_m, \mathbf{x}_{m'}), \tag{13}$$

where the "response matrix" (or transfer matrix)

$$\mathbf{K} = \sum_{n=1}^{N} q_n \mathbf{H}_n \mathbf{H}_n^T. \tag{14}$$

Elements of the matrix $\mathbf{K}$ are given by

$$K_{m,m'} = K(\mathbf{x}_m, \mathbf{x}_{m'}) = \sum_{n=1}^{N} q_n G_0(\mathbf{x}_m, \mathbf{y}_n) G_0(\mathbf{y}_n, \mathbf{x}_{m'}) \tag{15}$$

Clearly, the response matrix $\mathbf{K}$ is complex and symmetric.

3 Imaging and Inversion Using Linear Subspace Methods

One class of imaging methods available for time-reversal imaging of small targets may be called linear subspace methods, of which the best known method is probably MUSIC (Schmidt, 1979; Marple, 1987; Stoica and Nehoral, 1990; Xu and Kaveh, 1996; Stoica and Moses, 1997). The term MUSIC stands for MUltiple SIgnal Classification scheme. The method determines whether or not each vector in a set of vectors is fully or only partially in the range of an operator. If $\mathbf{T} = \mathbf{K}\mathbf{K}^*$ is the operator of interest (*i.e.*, the time-reversal operator), and the complete set of eigenvectors in the range of the operator (*i.e.*, having nonzero eigenvalue) is given by $\{\mathbf{V}_n\}$, then we can choose a test vector $\mathbf{H}_r$ [see (12)] and define the square of the direction cosine between $\mathbf{H}_r$ and any one eigenvector $\mathbf{V}_n$ to be

$$\cos^2(\mathbf{V}_n, \mathbf{H}_r) = |\mathbf{V}_n^{*T} \cdot \mathbf{H}_r|^2 / |\mathbf{H}_r|^2. \tag{16}$$

We are assuming in this formula that all the eigenvectors $\mathbf{V}_n$ are normalized so $|\mathbf{V}_n| = 1$, while $\mathbf{H}_r$ is not necessarily normalized.

3.1 MUSIC and variations

In the present application, $\mathbf{r}$ is a vector ranging over all or some discrete subset of the positions in the model space (usually a set of grid points). Then, there are several functionals we could plot in order to produce an "image" of the scatterers. The most common choice is the MUSIC classification functional

$$\csc^2(\{\mathbf{V_n}\},\mathbf{H}_r) = \frac{1}{1-\sum_{n=1}^{N}\cos^2(\mathbf{V_n},\mathbf{H}_r)}. \tag{17}$$

Another closely related possibility that has similar characteristics (but does not require normalization of $\mathbf{H}_r$ in some implementations) is

$$\cot^2(\{\mathbf{V_n}\},\mathbf{H}_r) = \frac{\sum_{n=1}^{N}\cos^2(\mathbf{V_n},\mathbf{H}_r)}{1-\sum_{n=1}^{N}\cos^2(\mathbf{V_n},\mathbf{H}_r)}. \tag{18}$$

The interpretation of these functionals as cosecants and cotangents in the subspaces determined by the eigenvectors should now be clear. By plotting these functionals, we find that the targets are located at those points where the denominators approach zero, and therefore in locations where the trial vector in entirely in the range of the scattering operator $\mathbf{K}$, or equivalently in the range of $\mathbf{T}$.

Now we can ask the question, how do we make use of these ideas if the data available to us are limited? In particular, it might happen that some of the nonzero eigenvalues are quite small compared to the others, and we do not know whether to include the corresponding eigenvectors in the set $\{\mathbf{V}_n\}$ or not. In this case, we can use a variation on the MUSIC scheme by only considering a subset of the eigenvectors, say $n = 1,\ldots,N' \leq N$. In this case, either of the two schemes just described is easily modified by restricting the sums to

$$\csc^2(\{\mathbf{V_n}\}',\mathbf{H}_r) = \frac{1}{1-\sum_{n=1}^{N'}\cos^2(\mathbf{V_n},\mathbf{H}_r)}, \tag{19}$$

and

$$\cot^2(\{\mathbf{V_n}\}',\mathbf{H}_r) = \frac{\sum_{n=1}^{N'}\cos^2(\mathbf{V_n},\mathbf{H}_r)}{1-\sum_{n=1}^{N'}\cos^2(\mathbf{V_n},\mathbf{H}_r)}. \tag{20}$$

This approach can then be used to test whether certain eigenvectors are really in the range or not by replotting these functions for different values of N'. The scheme just described could also be used to do crude imaging if only a single eigenvector is known, as might happen if we have used time-reversal processing in the time domain and had found only the first eigenvector.

When viewing eigenvectors as measurements, we see that using fewer eigenvectors will result in poorer resolution, as less information is then available to constrain the images.

3.2 Extended MUSIC for inversion

MUSIC as described so far is what I would call an "imaging method" in the sense that it is attempting to locate objects, but not to quantify their properties (such as the scattering strength q). We will show now that, with only a little more computational effort, we can also

determine the scattering coefficients. The resulting algorithm will then be distinguished as an "inversion method," rather than imaging.

Our data are again the matrix elements of the response matrix K. We know that K can be represented equally in two ways by its scattering expansion and its SVD so that

$$\mathbf{K} = \sum_{n=1}^{N} q_n \mathbf{H}_n \mathbf{H}_n^T = \sum_{m=1}^{M} \sigma_m \mathbf{V}_m \mathbf{V}_m^T, \tag{21}$$

recalling that there are M sensors in our array, N scatterers, and that the singular vectors are assumed to be normalized to unity.

One formulation of the inversion problem that is very similar in spirit to MUSIC is therefore to find a matrix

$$\tilde{\mathbf{K}} = \sum_{r=1}^{L^2} \tilde{q}_r \mathbf{H}_r \mathbf{H}_r^T, \tag{22}$$

whose elements agree with those of the measured K according to some criterion such as least-squares. The sum in (22) is taken over grid points in an $L \times L$ (pixel units) model space in 2D. Generalization to model spaces having other shapes and/or to 3D is straightforward, as there is no use made here of any symmetries in the choice of sensor array arrangement, or of the locations of the test pixels chosen as possible targets and indexed by r. We will want to take advantage of the orthogonality of the singular vectors $\mathbf{V}_m$. So we suppose that it is possible to solve an equation of the form

$$\sum_{r=1}^{L^2} \tilde{q}_r \mathbf{H}_r \mathbf{H}_r^T \simeq \sum_{m=1}^{M} \sigma_m \mathbf{V}_m \mathbf{V}_m^T, \tag{23}$$

in the least-squares sense for the coefficients $\tilde{q}_r$ associated with some set of points (pixel or voxel centers) in the model space.

Applying the singular vectors $\mathbf{V}_m^*$ to both the right and left sides of (23), we find

$$\sum_{r=1}^{L^2} \tilde{q}_r \left(\mathbf{H}_r^T \cdot \mathbf{V}_m^* \right)^2 = \sigma_m, \tag{24}$$

which can then be rewritten in matrix notation as

$$\begin{pmatrix} (\mathbf{H}_1^T \cdot \mathbf{V}_1^*)^2 & \dots & (\mathbf{H}_{L^2}^T \cdot \mathbf{V}_1^*)^2 \\ (\mathbf{H}_1^T \cdot \mathbf{V}_2^*)^2 & \dots & (\mathbf{H}_{L^2}^T \cdot \mathbf{V}_2^*)^2 \\ \vdots & \ddots & \vdots \\ (\mathbf{H}_1^T \cdot \mathbf{V}_M^*)^2 & \dots & (\mathbf{H}_{L^2}^T \cdot \mathbf{V}_M^*)^2 \end{pmatrix} \begin{pmatrix} \tilde{q}_1 \\ \tilde{q}_2 \\ \vdots \\ \tilde{q}_{L^2} \end{pmatrix} = \begin{pmatrix} \sigma_1 \\ \sigma_2 \\ \vdots \\ \sigma_M \end{pmatrix}. \tag{25}$$

We see that estimates of the coefficients can now be found by solving this rather large ($M \times L^2$) and underdetermined least-squares system. This form is similar to various kinds of tomography, with the singular values taking the role of the data, and the singular vectors taking the role of the discrete scanning modality. (For comparison, in traveltime tomography the data are the traveltimes, the matrix elements are the ray path lengths through the cells, and the model

parameters are the slownesses in the cells.) Note that the elements of the present matrix are in general complex, as are the scattering coefficients $\tilde{q}_r$, while the singular values σ_m are all nonnegative real numbers.

The computational situation can be improved significantly by noting the similarity of the matrix elements to the direction cosines already treated in MUSIC. In fact, if we take the magnitude of each matrix element, we have the square of a direction cosine. Furthermore, if we sum these magnitudes along the columns of the matrix, then we have obtained exactly the quantity

$$|\mathbf{H}_r|^2 \sum_{m=1}^{M} \cos^2(\mathbf{V}_m, \mathbf{H}_r), \tag{26}$$

which — except for the normalization factor $|\mathbf{H}_r|^2$ — is the sum over all the direction cosines associated with the vector $\mathbf{H}_r$. This column sum is therefore a measure of what we might call the "coverage" of the pixel centered at $\mathbf{r}$. If there is no coverage, this column sum is zero and the pixel does not contain a measurable target. If the normalized coverage is close to unity, then this pixel is one that MUSIC will clearly identify as a target. For intermediate values, the situation is somewhat ambiguous, as it is in the normal MUSIC algorithm, but clearly the closer the normalized sum is to unity, the more likely it is that the pixel contains a target.

Now we have a clear pixel selection criterion available, based on these column sums. Thus, we can reduce the size of the inversion problem posed in (25) very quickly by throwing out all pixels that have small column sums, and/or, equivalently, those whose values are $<< |\mathbf{H}_r|^2$. We can classify the remaining pixels by the magnitudes of the normalized sums, choosing to keep only (say) those pixels having the M largest normalized column sums. Or if there are clearly only $N << M$ singular values that are nonzero, then we could reduce the problem still further, and keep only those pixels having the N largest normalized column sums. If we have an $M \times M$ matrix when we have finished this selection process, then we can simply invert the matrix to find the values of the remaining $\tilde{q}$'s. If on the other hand, we have an $M \times N$ matrix that is not square remaining after this process of elimination, then we will again have to solve the inversion problem, by using overdetermined least-squares.

Another possibility when the singular values have a gradual fall off in magnitude as $m \to M$, but no precipitous drop to zero, is to multiply (25) on the left by a diagonal matrix whose nonzero elements are the singular values to some power p. Then, the resulting equation is

$$\sum_{r=1}^{L^2} \tilde{q}_r \sigma_m^p \left(\mathbf{H}_r^T \cdot \mathbf{V}_m^*\right)^2 = \sigma_m^{p+1}, \tag{27}$$

or, in vector/matrix notation,

$$\begin{pmatrix} \sigma_1^p(\mathbf{H}_1^T \cdot \mathbf{V}_1^*)^2 & \dots & \sigma_1^p(\mathbf{H}_{L^2}^T \cdot \mathbf{V}_1^*)^2 \\ \sigma_2^p(\mathbf{H}_1^T \cdot \mathbf{V}_2^*)^2 & \dots & \sigma_2^p(\mathbf{H}_{L^2}^T \cdot \mathbf{V}_2^*)^2 \\ \vdots & \ddots & \vdots \\ \sigma_M^p(\mathbf{H}_1^T \cdot \mathbf{V}_M^*)^2 & \dots & \sigma_M^p(\mathbf{H}_{L^2}^T \cdot \mathbf{V}_M^*)^2 \end{pmatrix} \begin{pmatrix} \tilde{q}_1 \\ \tilde{q}_2 \\ \vdots \\ \tilde{q}_{L^2} \end{pmatrix} = \begin{pmatrix} \sigma_1^{p+1} \\ \sigma_2^{p+1} \\ \vdots \\ \sigma_M^{p+1} \end{pmatrix}. \tag{28}$$

We can apply a MUSIC-like processing scheme to this matrix (that could then be called "weighted MUSIC$_p$" which is similar to some methods suggested by other authors). This approach permits the singular values to determine in a natural way the cutoff (if any) in the

contributions from those singular vectors of negligible importance to the inversion. For example, when $p = 2$, these column sums of the magnitudes of these elements are just $|\mathbf{K}^*\mathbf{H}_r|^2$, which is the matrix element of the time-reversal operator with vector $\mathbf{H}_r$.

4 Maximum-Entropy Imaging

4.1 Motivation

If we consider the structure of the response matrix K, whenever the number of targets is much less than the array size so that $N << M$, the matrix information is very redundant. The matrix is then rank N, where N is the number of targets to be imaged. Yet, the matrix K for M sensors in our array is $M \times M$, with $M(M+1)/2$ distinct complex elements. The total number of distinct data present is therefore $M(M+1)$, which is to be used to determine the x, y, z-coordinates in 3D of each target and possibly also its scattering strength q. For complex q, this means we need to find at most $5N$ numbers from $M(M+1)$. In the presence of noise or strong inhomogeneities in the background medium, the redundancy may be needed to resolve several or many targets. In homogeneous backgrounds, the overdetermined nature of this problem is something we need to consider.

Examples of situations in which limited data are available include: (1) Only one transducer is available. Assuming that the transducer is moveable, then it would be possible to collect data in a "synthetic aperture" mode as is commonly done in radar applications (SAR). (2) Only two transducers are available, but some triangulation is then possible. (3) Only one ping is allowed, but many transducers are available (multistatic case). Here, we can collect only one row of the response matrix. (4) Only the primary eigenvector has been found, as in iterative time-reversal processing in the physical domain, but no attempt has been made to find eigenvectors associated with secondary targets.

How much of the information in the scattering data is really needed to solve the inverse problem in these situations? With limited data, how much data is essential to collect to locate and possibly identify the targets of most interest?

Having posed the general problem, we will not try to answer it completely here. Instead, we will show some examples of what can be done to image with restricted data sets.

4.2 Maximum-entropy imaging

One approach to imaging with corrupted data or relatively small data sets is known as Maximum-Entropy Imaging (Gull and Daniell, 1978; Schmidt, 1979; Gull and Skilling, 1984). I will now describe this method briefly, although another method that is also based on the maximum entropy concept is the main focus of this section.

Perhaps the most common use of maximum-entropy imaging arises in astronomy, and especially in radioastronomy (Gull and Daniell, 1978). The goal is to find a map of the distribution of radio brightness across the sky. But the data collected and the methods used can produce a series of such maps, each having different resolutions and noise levels. There does not appear to be any preferred or "best" sky map associated with the data from this point of view. To resolve this ambiguity, we can choose to use an image that satisfies a maximum-entropy objective criterion (to be explained soon). The resulting maximum-entropy image should not be

thought of as the "true" map of the sky in this context, but rather as a map that does not lead to conclusions for which there is either very little or no evidence in the data. The analogy to our problem in acoustics of finding relatively isolated targets in an otherwise homogeneous background is also apparent.

The reader interested in understanding the general context of entropy and its role in statistical mechanics and information theory would do well to read the paper by Jaynes (1957). The history of maximum-entropy in astronomy is also beyond our scope here, but I will point out that Gull and Daniell (1978) introduced this algorithm in part as an alternative to the CLEAN algorithm (Högbom, 1974), which is another popular imaging algorithm (although not as popular now as is the maximum-entropy approach) for use with incomplete and noisy data.

Following Gull and Daniell (1978), we define an intensity m_{ij} at the pixel in the (i,j) position of a test map and let $\hat{m}_{kl}$ be the Fourier transform of m_{ij}. Then, suppose further that the data come to us in the form of measurements $\hat{n}_{kl}$ of the Fourier transform $\hat{m}_{kl}$. Assuming that these measurements have Gaussian errors, with standard deviations σ_{kl}, the data fitting part of the algorithm is a weighted least-squares error term of the form $\sum_{kl} |\hat{m}_{kl} - \hat{n}_{kl}|^2/\sigma_{kl}^2$. The objective constraint applied is that the entropy functional ($S = -\sum_{ij} m_{ij} \ln m_{ij}$), determined by the nonnegative intensities in the final map, is a maximum. This maximum-entropy objective is natural for imaging a sparsely occupied field because it corresponds to a situation where all the intensities have the same value, thus, providing a sky map with no information in the absence of data. Using these two terms to form an overall objective functional, including a Lagrange multiplier for the data constraints, gives

$$Q(m_{ij}, \lambda) \equiv -\sum_{ij} m_{ij} \ln m_{ij} - \frac{\lambda}{2} \sum_{kl} |\hat{m}_{kl} - \hat{n}_{kl}|^2/\sigma_{kl}^2. \tag{29}$$

One advantage of the second sum in Q is that it satisfies a χ^2 distribution, and, therefore, the value of this sum can be used as a measure of goodness of the data fit. In particular, the expected value of the sum is equal to the number of terms in the sum. The disadvantage of this sum is that it requires prior knowledge of the standard deviations. For other imaging problems, the second term in (29) could be replaced by an output least-squares functional together with a tolerance criterion as in Morozov's discrepancy principle (Morozov, 1967; 1984; Tikhonov and Arsenin, 1979; Groetsch, 1984; Hanke, 1997; Haber *et al.*, 2000).

We will not pursue this approach further here, but instead introduce another approach that makes use of the maximum-entropy imaging concept.

4.3 A new maximum-entropy imaging method

We assume that a set of data has been produced using active sources, that the time series response has been measured as a time series, and that these data have been Fourier transformed to produce the response matrix. At this point, there are two possibilities: (1) We could make direct use of the response matrix, or (2) we could continue processing the data by forming the time-reversal matrix and then computing the eigenvectors of the matrix. A third possibility that will be seen as a special case of the previous ones is that time-reversal data is collected and a single eigenvector is constructed by iteration on the physical system.

For our present purposes, in any of these cases we can take the diagonal entries of the response matrix as our data, or the diagonal entries of the rank one matrix formed from any

eigenvector (computed or measured directly) of the time-reversal matrix as our data. We assume at first that there is a single target present. Then, for the eigenvectors, the diagonal entries will be real and positive numbers, but they will all contain a constant normalization factor associated with the norm of the eigenvector. For the response matrix, the diagonal entries will be complex and contain a constant factor associated with the scattering strength of the target. We eliminate the unit magnitude phase factor in response matrix diagonals by taking the magnitudes of these entries. Then, we see that in all the cases considered these diagonal data have (for homogeneous 3D media) the form

$$f_n = \frac{\gamma_i}{(4\pi)^2|\mathbf{r}_n - \mathbf{r}_i|^2} \qquad \text{for} \qquad n = 1, \ldots, N, \tag{30}$$

where γ_i is the magnitude of the scattering strength for the response matrix data, or the norming constant for the eigenvector data. The location of the target is $\mathbf{r}_i$ and the location of the nth element of the acoustic array (having a total of N elements) is $\mathbf{r}_n$.

Using these data, we want to construct a figure of merit that will identify the target location by producing either a noticeably high or a noticeably low value for any point in the imaging region to scanned. To accomplish this, we form the numbers

$$\phi_n(\mathbf{r}) = f_n(4\pi)^2|\mathbf{r} - \mathbf{r}_n|^2 \tag{31}$$

where $\mathbf{r}$ is the location of any point in the imaging region. Then, we see that when $\mathbf{r} = \mathbf{r}_i$ is located at or very near to the target, then

$$\phi_n(\mathbf{r}_i) = \gamma_i \tag{32}$$

for all N functions ϕ_n. So we want to construct a figure of merit that gives special significance to functions that are positive and constant. But it is precisely this feature that distinguishes the maximum-entropy approach to imaging. If we define an entropy functioinal H such that

$$H(p_1, \ldots, p_N) = -k \sum_{n=1}^{N} p_n \ln p_n, \tag{33}$$

with the constraint that the probabilities $p_n \geq 0$ and $\sum p_n = 1$, then we construct a maximum principle based on the cst or objective functional

$$J(p_1, \ldots, p_N, \lambda) = H(p_1, \ldots, p_N) + \lambda(\sum p_n - 1), \tag{34}$$

where λ is the Lagrange multiplier for the constraint. The minimum occurs when the constraint is satisfied, and when

$$p_n = e^{(\lambda - 1)/k} \qquad \text{for all} \qquad n = 1, \ldots, N. \tag{35}$$

Thus, the maximum entropy occurs when all N states are equally probable.

We can turn this useful fact into an imaging principle by making a small modification in the foregoing derivation. If we define

$$p_n = \phi_n / \Phi \tag{36}$$

where $c \equiv \sum_n \phi_n$, we see that the maximum-entropy functional can be used as a means of identifying spatial locations at which the various ϕ_n values converge to a constant. The constant k is not important for this application and can be taken as unity. The value of the Lagrange multiplier at the maximum can be determined using (32) and (35) to be

$$\lambda = 1 + \ln(\gamma_i/c) = 1 - \ln(N), \tag{37}$$

since $c = N\gamma_i$ at the target location. Near the maximum of J, we can approximate it in either of two ways:

$$J \simeq -\frac{1}{N}\sum_n \left(\frac{\phi_n}{\gamma_i} - 1\right)^2 = 1 - \frac{1}{N}\sum_n \left(\frac{\phi_n}{\gamma_i}\right)^2$$

or

$$J \simeq -\frac{1}{N}\sum_n \left[\ln\left(\frac{\phi_n}{\gamma_i}\right)\right]^2. \tag{38}$$

For our present purposes, the second of these forms has proven to be somewhat preferable over the other. The normalizing constant N in this expression has no effect on the result, and whether we look for the minimum or maximum of our function is an arbitrary choice, so we can choose instead to study

$$\tilde{J} \equiv \sum_n \left[\ln\left(\frac{\phi_n}{\gamma_i}\right)\right]^2. \tag{39}$$

which still requires that we know the scattering strength or norming constant γ_i, which we may or may not know.

If we know γ_i, then we can image the target using (39) directly. If we do not know γ_i, then we need an estimate of it. One convenient way of obtaining an estimate is by picking any one of the ϕ_n values as the estimate. Clearly, this choice gives a good approximation to the right result at the target, but it will also cause some smearing of the image. The imaging algorithm in this case is then based upon

$$\tilde{J}_q \equiv \sum_n \left[\ln\left(\frac{\phi_n}{\phi_q}\right)\right]^2, \tag{40}$$

where q is any one of the values $n = 1, \ldots, N$. This approach works and gives the results shown in Figures 3 and 4. In these Figures, we chose q to be the transducer coordinate of the one that measured the largest amplitude of all the transducers. We see that the results are a little peculiar in the sense that the region of disturbed values near the target location has a teardrop shape, and the center of the teardrop also has some curvature directed away from the center of the array. This observation suggests that it might be preferable not to make any particular choice of q, but instead to consider them all equally. We can do so by symmetrizing the result as much as possible with data available, and also possibly sharpen the image. This criterion results in the imaging objective functional

$$\tilde{J} \equiv \sum_n \left[\ln\left(\frac{\phi_n}{\phi_q}\right)\right]^2 \tag{41}$$

The result of using this criterion is shown in Figure 5, which should be compared directly to Figure 4.

To understand a little better what this symmetrized maximum-entropy imaging scheme is doing to map the data into an image, we will expand (41) so that

$$\begin{aligned}\hat{J} &= \sum_{n,q}[\ln\phi_n - \ln\phi_q]^2 \\ &= 2\left[\sum_{n,q}(\ln\phi_n)^2 - \sum_n \ln\phi_n \sum_q \ln\phi_q\right] \\ &= 2\left[N\sum_n(\ln\phi_n)^2 - \left(\sum_n \ln\phi_n\right)^2\right] \end{aligned} \tag{42}$$

By defining an averaging operator over the functional values at the locations of the N transducers such that $< \cdot >\equiv \frac{1}{N}\sum\cdot$, we see that (42) is of the form

$$\hat{J} = 2N^2\left[< |\ln\phi|^2 > - < |\ln\phi| >^2\right] \tag{43}$$

and therefore shows that $\hat{J}$ is a measure of the fluctuations in $|\ln\phi|$ at each location in the region being mapped. At the target location, the fluctuations vanish identically, since they become equal to the constant $\ln\gamma_i$. Equation (43) is very useful for two reasons: (1) it shows how the modified maximum entropy imaging criterion is related to fluctuations in ϕ, and (2) it points out that the form $\hat{J}$ could have been postulated as our imaging criterion in the first place, independent of the derivation provided here, since it uses exactly the same features of the data to distinguish the location of the target.

5 Conclusions

After describing a well-known method in radio astronomy called maximum-entropy imaging, I introduced a new method that also uses the maximum-entropy concept but in another way. The main distinction between these two approaches is that the well-known approach uses the entropy functional as a means of regularizing the data inversion in order to produce well-resolved images of point objects – stars in the case of radio astronomy. The new method uses the entropy functional not as a smoother or regularizer, but rather as the imaging criterion. When the entropy functional is maximum, or equivalently when our modified functional vanishes at some point in space, that is the location of a target. By plotting the inverse of this modified functional, we arrive at a method that has much in common with the MUSIC algorithm for imaging, but the new method uses different data. MUSIC requires the computation of the SVD of the response matrix. The new method can make use of this information if available, but does not require it. Furthermore, the new method can make use of just the diagonal elements of the response matrix (as in synthetic aperture imaging), or it can be used with time domain amplitude data for the main arrivals.

Future work on this approach will explore how robust the method is when the propagating medium is itself random, in addition to the presence of the isolated scatterers/targets we want to localize.

Acknowledgments

I benefited greatly from discussions of these and related imaging methods with Liliana Borcea, George Papanicolaou, Chrysoula Tsogka, and Michael Vogelius. Work performed under the auspices of the U. S. Department of Energy by the University of California Lawrence Livermore National Laboratory under contract No. W-7405-ENG-48 and supported specifically by the LLNL Laboratory Directed Research and Development Program and the Environmental Management Sciences Program.

References

P. Blomgren, G. C. Papanicolaou, and H. Zhao, Super-resolution in time-reversal acoustics, *J. Acoust. Soc. Am.*, to appear, 2001.

M. Brühl, M. Hanke, and M. S. Vogelius, A direct impedance tomography algorithm for locating small inhomogeneities, preprint (2001).

D. H. Chambers and A. K. Gautesen, Time reversal for a single spherical scatterer, *J. Acoust. Soc. Am.* **109**, 2616–2624 (2001).

E. Cherkaeva and A. C. Tripp, Optimal survey design using focused resistivity arrays, *IEEE Trans. Geosci. Remote Sensing* **34**, 358–366 (1996a).

E. Cherkaeva and A. C. Tripp, Inverse conductivity problem for inexact measurements, *Inverse Problems* **12**, 869–883 (1996b).

D. Colton and A. Kirsch, A simple method for solving inverse scattering problems in the resonance region, *Inv. Prob.* **12**, 383–393 (1996).

A. J. Devaney, Super-resolution processing of multi-static data using time reversal and MUSIC, preprint, 1999.

M. Fink, Time reversal acoustics, *Physics Today* **50**, 34–40 (March, 1997).

M. Fink, Time-reversed acoustics, *Scientific American* **281**, 91–97 (November, 1999).

D. G. Gisser, D. Isaacson, and J. C. Newell, Electric current computed tomography and eigenvalues: *SIAM J. Appl. Math.* **50**, 1623–1634 (1990).

C. W. Groetsch, *Theory of Tikhonov Regularization for Fredholm Equations of the First Kind* (Pitman, Boston, Massachusetts, 1984).

S. F. Gull and G. J. Daniell, Image reconstructin from incomplete and noisy data, *Nature* **272**, 686–690 (1978).

S. F. Gull and J. Skilling, Maximum entropy imaging method in image processing, *IEE Proc. – Part F. Commun., Radar, Signal Proc.* **131**, 646–659 (1984).

E. Haber, U. M. Ascher, and D. Oldenburg, On optimization techniques for solving nonlinear inverse problems, *Inverse Problems* **16**, 1263–1280 (2000).

M. Hanke, A regularizing Levenberg-Marquardt scheme with applications to Inverse groundwater filtration problems, *Inverse Problems* **13**, 79–95 (1997).

J. A. Högbom, Aperture synthesis with a non-regular distribution of interferometer baselines, *Astron. Astrophys. Suppl.* **15**, 417–426 (1974).

D. Isaacson, Distinguishability of conductivities by electric current computed tomography, *IEE Trans. Med. Imaging* **MI-5**, 91–95 (1986).

E. T. Jaynes, Information theory and statistical mechanics, *Phys. Rev.* **106**, 620–630 (1957).

A. Kirsch, Characterization of the shape of a scattering obstacle using the spectral data of the far field operator, *Inv. Prob.* **14**, 1489–1512 (1998).

S. L. Marple, *Digital Spectral Analysis* (Prentice-Hall, Englewood Cliffs, NJ, 1987), pp. 373–378.

T. D. Mast, A. I. Nachman, and R. C. Waag, Focusing and imaging using eigenfunctions of the scattering operator, *J. Acoust. Soc. Am.* **102**, 715–725 (1997).

V. A. Morozov, On the solution of functional equations by the method of regularization, *Sov. Math. Doklay* **7**, 414–417 (1967).

V. A. Morozov, *Methods for Solving Incorrectly Posed Problems* (Springer, New York, 1984).

C. Prada and M. Fink, Eigenmodes of the time reversal operator: A solution to selective focusing in multiple-target media, *Wave Motion* **20**, 151–163 (1994).

C. Prada, J.-L. Thomas, and M. Fink, The iterative time reversal process: Analysis of the convergence, *J. Acoust. Soc. Am.* **97**, 62–71 (1995).

C. Prada, F. Wu, and M. Fink, The iterative time reversal mirror: A solution to self-focusing in the pulse echo mode, *J. Acoust. Soc. Am.* **90**, 1119–1129 (1991).

R. O. Schmidt, Multiple emitter location and signal parameter estimation, *Proc. RADC Spectrum Estimation Workshop*, Rome Air Development Center, Rome, NY, RADC-TR-79-63, October, 1979, pp. 243–258; reprinted in *IEEE Trans. Antennas Prop.* **AP-34**, 276–280 (1986).

P. Stoica and R. L. Moses, *Introduction to Spectral Analysis* (Prentice-Hall, Englewood Cliffs, NJ, 1997).

P. Stoica and A. Nehoral, MUSIC, maximum likelihood, and Cramér-Rao bound: Further results and comparisons, *IEEE Trans. Acoustics, Speech, and Signal Proc.* **38**, 2140-2150, 1990.

A. N. Tikhonov and V. Ya. Arsenin, *Methods for Solving Ill-Posed Problems* (Wiley, New York, 1979).

C. Tsogka and G. C. Papanicolaou, Time reversal through a solid-liquid interface and super-resolution, *J. Acoust. Soc. Am.* , submitted, 2001.

W. Xu and M. Kaveh, Comparative study of the biases of MUSIC-like estimators, *Signal Processing* **50**, 39–55, 1996.

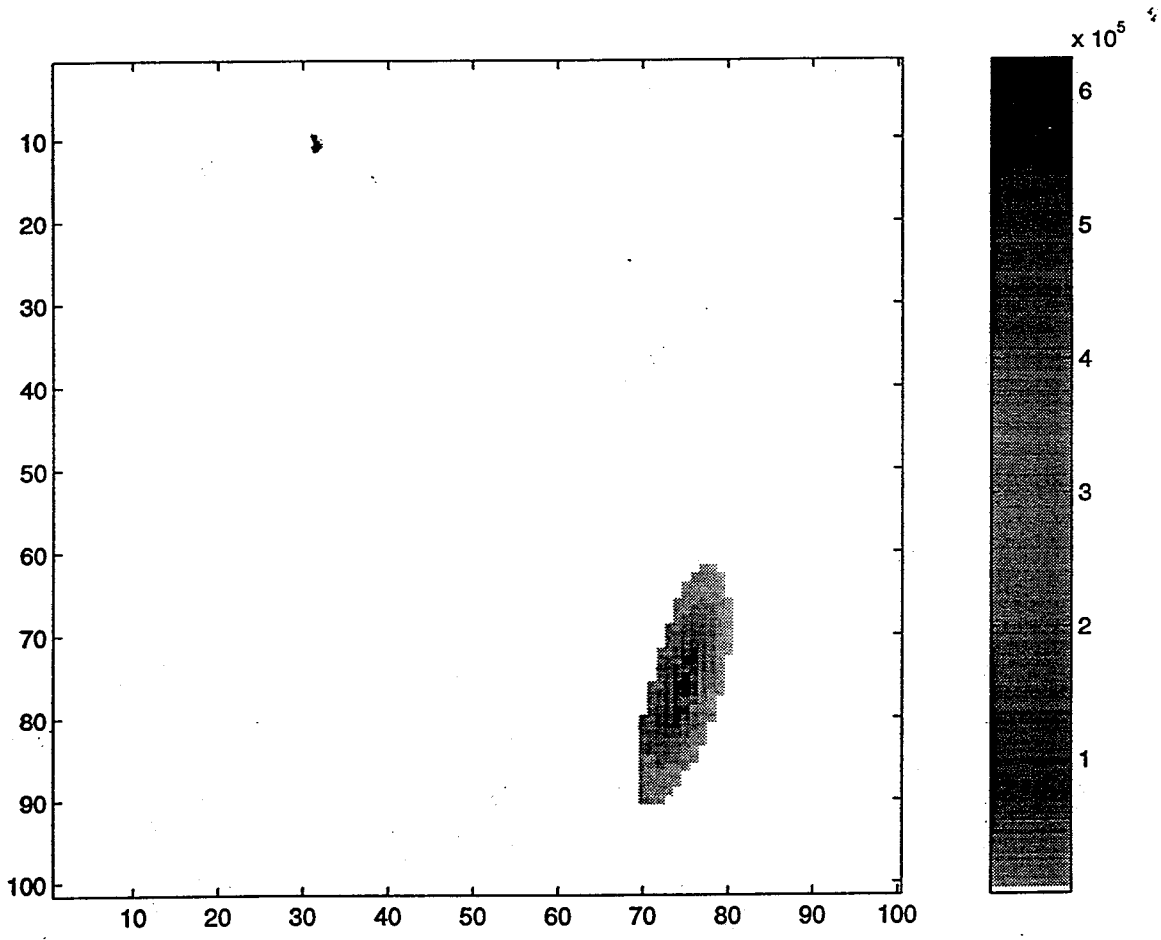

Figure 1: Time-reversal imaging for a single target using (38).

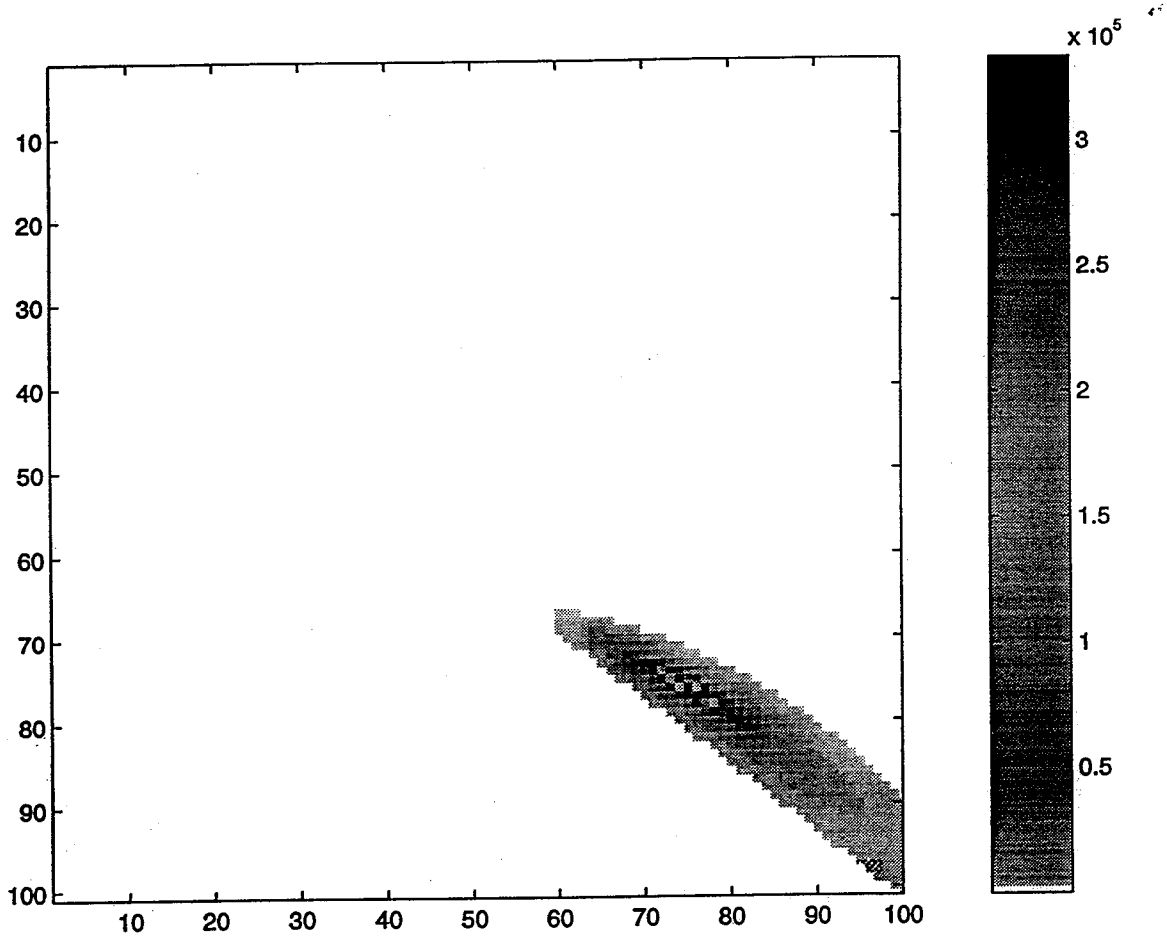

Figure 2: Response matrix imaging for a single target using (39).

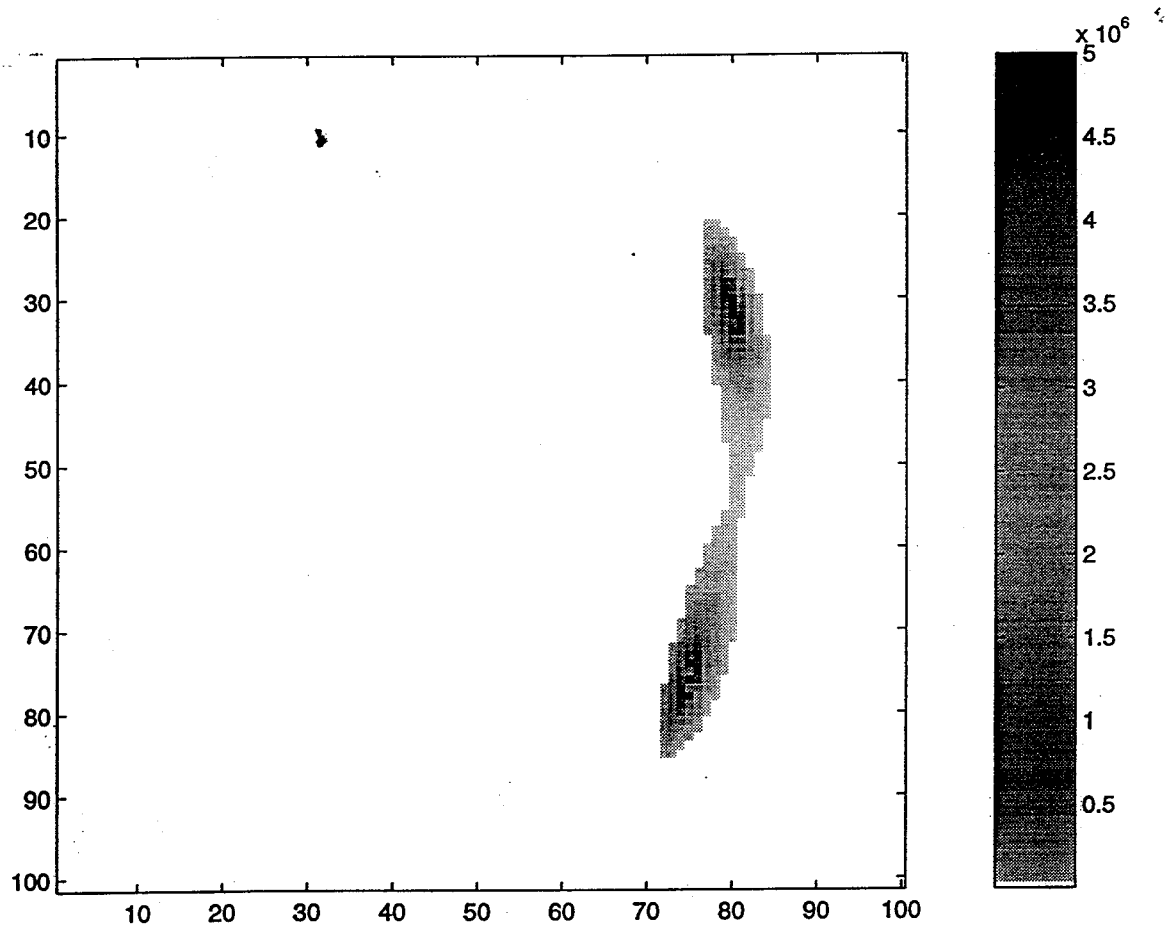

Figure 3: Time-reversal imaging for two targets using (38).

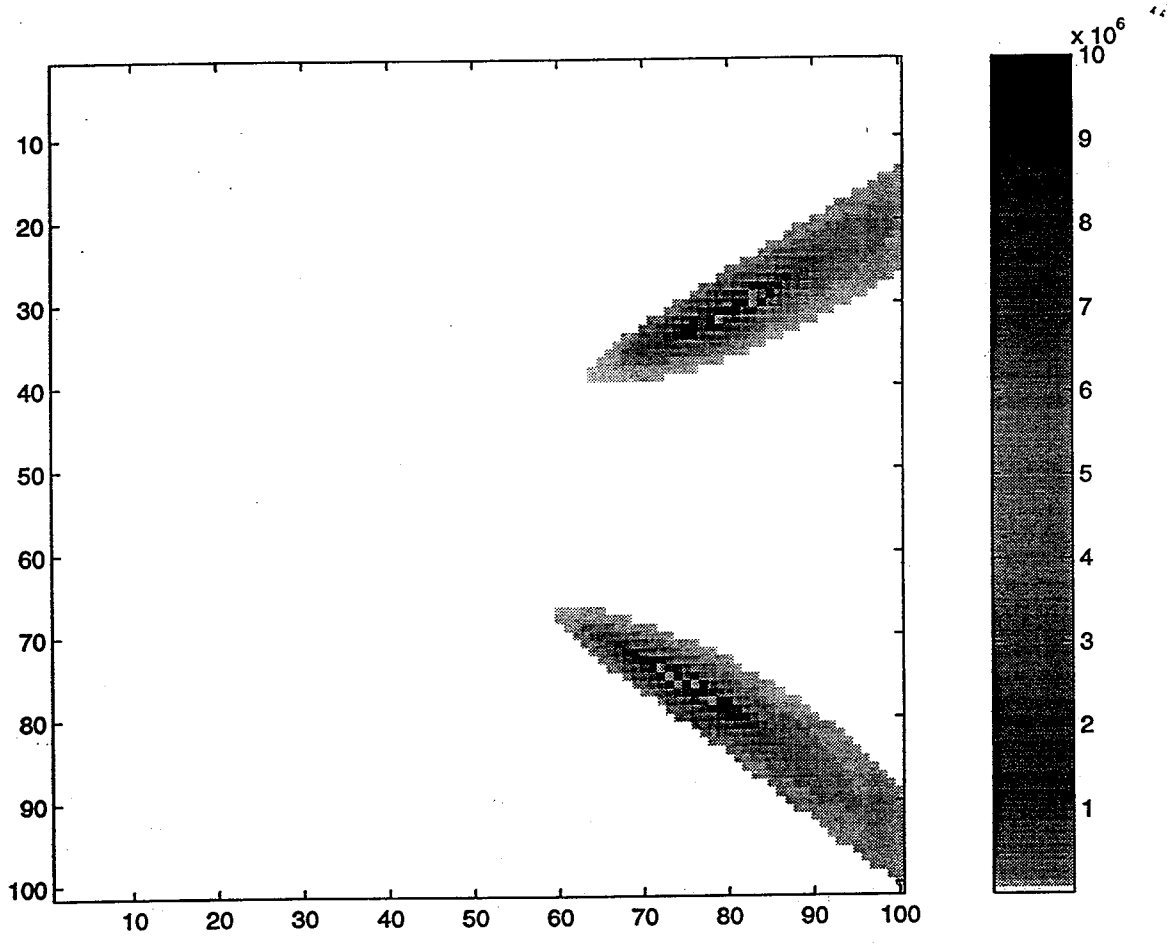

Figure 4: Response matrix imaging for two targets using (39).

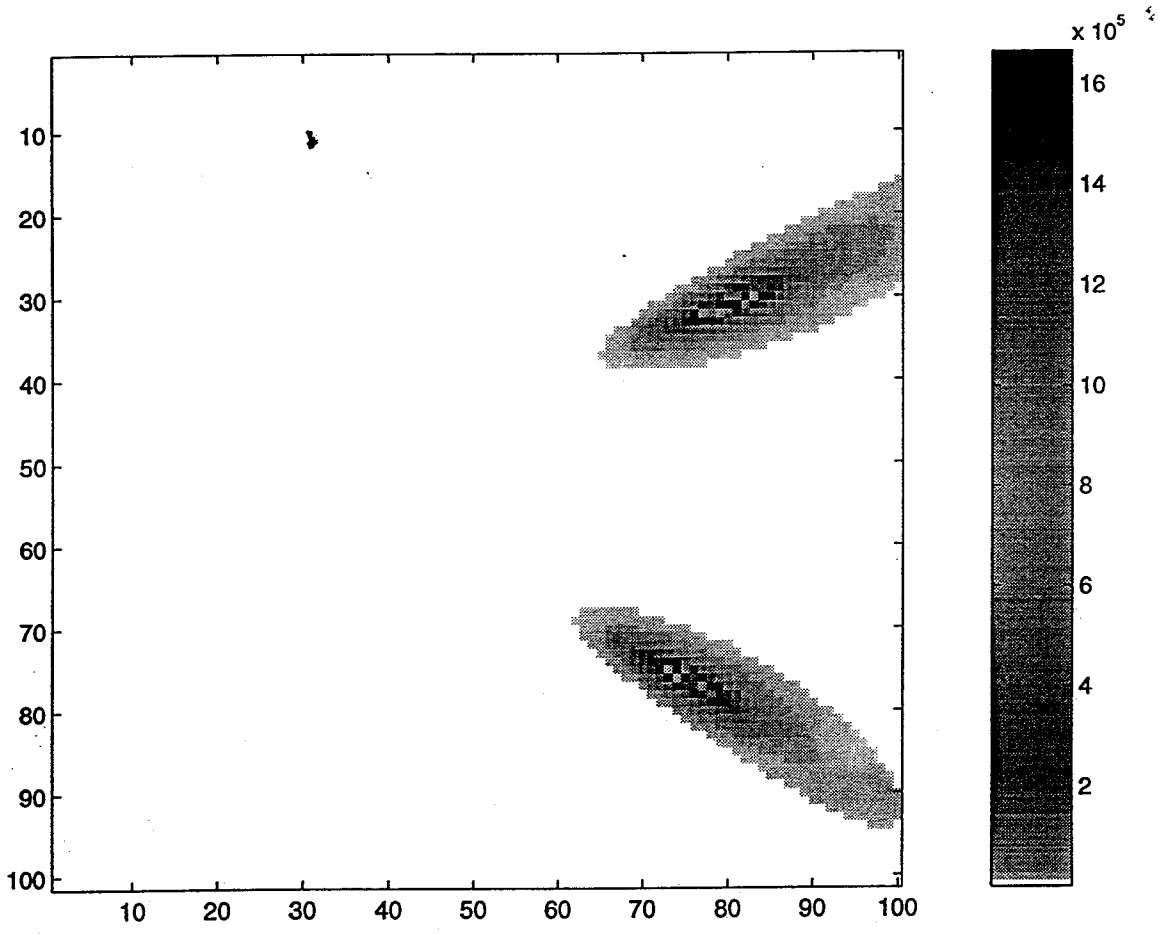

Figure 5: Response matrix imaging for two targets using (40).

University of California
Lawrence Livermore National Laboratory
Technical Information Department
Livermore, CA 94551